ChemPubSoc Europe

DOI: 10.1002/open.201500031

Open Access ChemistryOPEN Communications

Lithium Insertion Mechanism in Iron-Based Oxyfluorides with Anionic Vacancies Probed by PDF Analysis

Damien Dambournet,*[a, b] Karena W. Chapman,[c] Mathieu Duttine,[a, b, d] Olaf Borkiewicz,[c] Peter J. Chupas,[c] and Henri Groult[a, b]

The mechanism of lithium insertion that occurs in an iron oxyfluoride sample with a hexagonal–tungsten–bronze (HTB)-type structure was investigated by the pair distribution function. This study reveals that upon lithiation, the HTB framework collapses to yield disordered rutile and rock salt phases followed by a conversion reaction of the fluoride phase toward lithium fluoride and nanometer-sized metallic iron. The occurrence of anionic vacancies in the pristine framework was shown to strongly impact the electrochemical activity, that is, the reversible capacity scales with the content of anionic vacancies. Similar to FeOF-type electrodes, upon de-lithiation, a disordered rutile phase forms, showing that the anionic chemistry dictates the atomic arrangement of the re-oxidized phase. Finally, it was shown that the nanoscaling and structural rearrangement induced by the conversion reaction allow the in situ formation of new electrode materials with enhanced electrochemical properties.

In the context of lithium batteries, the discovery by Poizot et al.[1] of conversion reactions that occur when metal oxides such as CoO are used as electrode materials, has led to enthusiastic research activities.[2–4] Indeed, the electrochemical mechanism of these compounds, denoted MX_n, in which M is the metal and X is oxygen or fluorine, is characterized by a multistep electron-transfer process. Consequently, the occurrence of conversion reactions allows one to obtain high energy densities.

During the discharge (reduction) process, the metallic compound can be reduced with full use of all the redox potentials of the host metal. This reduction process leads to atomic rearrangement with the destruction of the parent crystal structure, yielding metallic nanoparticles embedded in a LiX lithiated matrix. The size of the metal nanoparticles ranged from 1 to 3 nm and remained throughout the reduction reaction.[5] This feature has been rationalized by considering interface chemistry between the parent structure, the metallic cluster, and the lithiated phase. As long as the reaction proceeds, the stress that occurs at the interface is better accommodated by favoring nanoscale rather than particle growth.[6] Moreover, the metal can form an interconnected and porous network, providing a pathway for electron transport.[7,8]

During the charge process, the oxidation of metallic nanoclusters occurs, leading to nanoparticles with unique properties. For instance, nanostructured RuO_2 has been synthesized by using a conversion process.[9] The discharge reaction first generates a metal/Li_2O nanocomposite, which was subsequently charged to obtain a nanostructured metal oxide. Owing to nanoscale features, the RuO_2 electrochemically prepared via this process showed enhanced supercapacitance performance.

Regardless of the compound used as the electrode material, the structure and composition of the re-oxidized phase can deviate from the pristine phase. Probing the structure and composition of the newly formed compound is very challenging, as both finite-size effects and amorphization induce an absence of long-range order. As a result, the use of conventional X-ray diffraction methods are precluded.

The presence of several anions in the original lattice contributed to the complexity of the overall atomic rearrangement. The incorporation of oxygen within the fluorinated network was introduced as a way to improve the intrinsic electronic conductivity, one of the major counterparts of using metal fluoride.[10] As a result, electrochemical tests performed on FeOF showed improved properties with respect to pure fluoride.[11] Nevertheless, the lithium storage mechanism occurring in FeOF is a typical example in which the "active" material differs from the parent phase.[12] Through the use of a combined in situ pair distribution function (PDF) and NMR analyses, it has been shown that the conversion of FeOF induced a partitioning of anions, resulting in a fluorine-rich amorphous rutile phase and an oxygen-rich rock salt phase. Such an anionic partitioning phenomenon has also been observed in a titanium-based hydroxyfluoride.[13]

Recently, iron hydroxyfluoride $FeF_{2.2}(OH)_{0.8}$ with a hexagonal–tungsten–bronze (HTB) network was synthesized by using a microwave-assisted precipitation method.[14] The partial dehydroxylation of the structure performed by an adequate thermal treatment enables the stabilization of anionic vacancies (□) in the HTB framework, yielding $FeF_{2.2}(OH)_{0.8-x}O_{x/2}□_{x/2}$ composi-

[a] Dr. D. Dambournet, Dr. M. Duttine, Dr. H. Groult
Sorbonne Universités, UPMC, Univ. Paris 06, UMR 8234, PHENIX, 75005 Paris (France)
E-mail: damien.dambournet@upmc.fr

[b] Dr. D. Dambournet, Dr. M. Duttine, Dr. H. Groult
CNRS, UMR 8234, PHENIX, 75005 Paris (France)

[c] Dr. K. W. Chapman, Dr. O. Borkiewicz, Dr. P. J. Chupas
X-ray Science Division, Advanced Photon Source
Argonne National Laboratory, Argonne, IL 60439 (USA)

[d] Dr. M. Duttine
CNRS, Univ. Bordeaux, ICMCB, UPR 9048, 33600 Pessac (France)

tion. Remarkably, the stabilization of anionic vacancies significantly improves the electrochemical properties.

The electrochemical insertion of Li^+ performed up to 2 V, in a $FeF_{2.2}(OH)_{0.8-x}O_{x/2}\square_{x/2}$ electrode, was shown to induce a drastic amorphization of the structure. De-insertion of lithium up to 4.2 V has enabled to recover weak structural features of the HTB-type structure, which led us to suggest that this compound is stable upon lithium insertion. This hypothesis was also supported by ex situ X-ray diffraction analysis performed on the defect-free compound, i.e., $FeF_3{\cdot}(H_2O)_{0.33}$.[15]

In this study, by means of PDF, a unique method to probe local–intermediate-range order,[16] we thoroughly investigated the lithium insertion mechanism that occurs in $FeF_{2.2}(OH)_{0.8-x}O_{x/2}\square_{x/2}$ electrodes with varied contents of anionic vacancies. In contrast to our previous suggestion, the results clearly show that at the early stage of the electrochemical lithium insertion, the HTB structure collapses via anionic partitioning with stabilization of fluoride- and oxide-rich phases. The fluoride phase is subsequently converted into metallic iron and lithium fluoride. Such a behavior is similar to FeOF-type electrodes, highlighting the role of anionic chemistry in conversion-based reactions. Strikingly, when used in the 2–4.2 V voltage range, the electrochemically synthetized composite showed improved redox properties with higher capacity and output voltage than the pristine compound, emphasizing the beneficial role of nanoscale features induced by conversion mechanisms.

Two samples of $FeF_{2.2}(OH)_{0.8-x}O_{x/2}\square_{x/2}$ with different amounts of anionic vacancies were prepared by thermal treatment of $FeF_{2.2}(OH)_{0.8}$ at 300 and 350 °C under argon. Mössbauer spectroscopy showed the presence of 12 and 15% of iron in five-fold coordination for the sample prepared at 300 and 350 °C, respectively. The sample prepared at 350 °C contains a small amount of amorphous iron oxide, as shown by PDF analysis and Mössbauer.[14]

The galvanostatic discharge/charge curves obtained for $FeF_{2.2}(OH)_{0.8-x}O_{x/2}\square_{x/2}$ electrodes are given in Figure 1 and compared with the pristine material, $FeF_{2.2}(OH)_{0.8}$. It is shown that the occurrence of anionic vacancies significantly improves the electrochemical activity of iron-based electrodes both within the 2 V and 1 V regions. Moreover, the reversible capacity scales with the content of anionic vacancies.

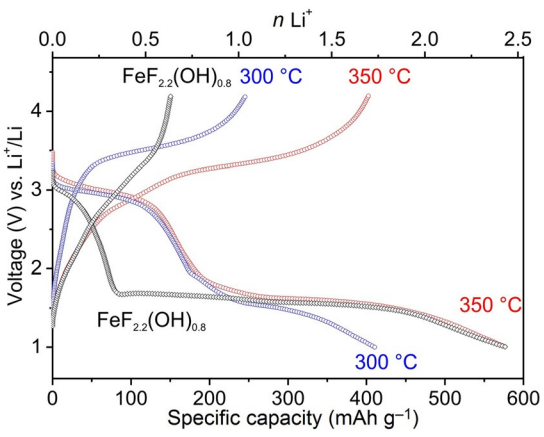

Figure 1. Initial discharge and charge curves obtained for $FeF_{2.2}(OH)_{0.8}$ and $FeF_{2.2}(OH)_{0.8-x}O_{x/2}\square_{x/2}$ electrodes prepared by thermal treatment at 300 and 350 °C. Cells were cycled under 50 mA g^{-1}.

At the early stage of the discharge, $FeF_{2.2}(OH)_{0.8-x}O_{x/2}\square_{x/2}$ electrodes exhibit a plateau region at ~3 V followed by a rapid decay in the potential down to 1.5–1.6 V, yielding to the reaction of about one lithium per iron. The reaction potential supports the reduction reaction of Fe^{3+} to Fe^{2+}.[11] Thereafter, the voltages are characteristic of the conversion regime, which is usually marked by a plateau region. The pristine $FeF_{2.2}(OH)_{0.8}$ material shows a large plateau occurring at 1.6 V but with poor reversibility. $FeF_{2.2}(OH)_{0.8-x}O_{x/2}\square_{x/2}$ electrodes show a smooth transition toward conversion, with a plateau region whose length depends on the anionic vacancy content. The sample prepared at 350 °C displays the highest capacity, with 580 mAh g^{-1} (2.43 Li^+). The $FeF_{2.2}(OH)_{0.8-x}O_{x/2}\square_{x/2}$ electrode, with the lowest content of anionic vacancies, presents a lower discharge capacity of 410 mAh g^{-1}. Upon re-oxidation, the charge capacities are 245 and 400 mAh g^{-1} for the sample prepared at 300 and 350 °C, respectively. Strikingly, three domains can be distinguished on the charge curve of the sample prepared at 350 °C, that is, a rapid increase in the voltage up to 2.7 V, followed by a smooth increase to ~3.2 V, and finally a plateau region.

The lithium insertion mechanism in $FeF_{2.2}(OH)_{0.8-x}O_{x/2}\square_{x/2}$ electrodes was first studied for reactions up to 1 Li^+ corresponding to the reduction of Fe^{3+} to Fe^{2+}. PDFs of $FeF_{2.2}(OH)_{0.8-x}O_{x/2}\square_{x/2}$ electrodes were obtained at intermediate states of discharge: 0.25, 0.5, 0.75, and 1 Li^+ per Fe. For each composition, attempt to fit the PDF was performed using different structural models. Best fits (Figure 2a) were obtained for a lithium insertion mechanism involving an anionic partitioning, yielding fluoride- and oxygen-rich phases. In addition, PDF refinements enabled the drawing of a phase analysis (Figure 2b), emphasizing complex atomic changes during the Fe^{3+}/Fe^{2+} reduction reaction.

At 0.25 Li, the PDF was successfully modeled by the initial HTB structure (Figure 2c) with substantial unit cell volume change from 701 to ~722 $Å^3$, indicating lithium insertion within the framework. After the insertion of 0.5 Li^+ corresponding to the end of the first plateau, an amorphous FeF_2 rutile-like phase was detected with optimized coherently PDF scattering domains of ~10 Å, revealing disorder. Moreover, the addition of a rock salt phase improves the fit with a reliability factor (R_w) going from 27.2 to 22.7%, consistent with an anionic partitioning phenomenon. From 0.5 to 1 Li^+, refinements (Figure 2b) indicate that the rock salt phase is continuously growing and is converted from the pristine HTB phase which suggests the presence of fluoride ions within the rock salt phase (Li–Fe–O–F). The formation of a rock salt phase containing fluoride has also been suggested to occur during the sodiation of $FeO_{0.7}F_{1.3}$/C electrode.[17] Moreover, an increasing disorder during the rock salt's growth was observed which can be related to the presence of fluoride, and/or increasing lithium content within the network. Note that after insertion of one lithium, a small amount of HTB was still detected due to incomplete reaction.

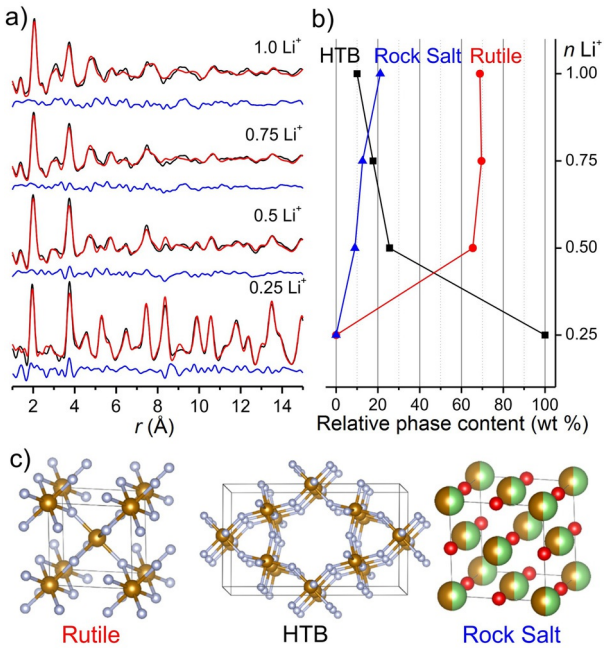

Figure 2. a) Fits of the PDF of $Li_nFeF_{2.2}(OH)_{0.8-x}O_{x/2}\square_{x/2}$ electrodes at various states of discharge: 0.25, 0.5, 0.75, and 1 Li^+ per Fe; the reliability factors (R_w) are 19, 22.7, 24.2, and 25.7% for 0.25, 0.5, 0.75, and 1 Li^+, respectively. b) Quantitative phase analysis from PDF refinements. c) Structural representation of the three phases used for the fits.

Beyond one lithium per iron, the occurrence of a conversion process characterized by a plateau region at ~1.6 V was confirmed by analyzing PDFs of discharged $FeF_{2.2}(OH)_{0.8-x}O_{x/2}\square_{x/2}$ electrodes to 1 V. The fit to the PDF data unambiguously reveals the conversion of the amorphous rutile FeF_2 toward Fe^0 and LiF. Figure 3 shows the fit to the PDF of the discharged $FeF_{2.2}(OH)_{0.8-x}O_{x/2}\square_{x/2}$ electrode prepared at 350 °C (R_w = 16.3%). The fit was performed using a three-phase refinement including a rock salt $Li_xFe_{1-x}O$, LiF, and metallic Fe. The lower discharge capacity observed for $FeF_{2.2}(OH)_{0.8-x}O_{x/2}\square_{x/2}$ prepared at 300 °C was attributed to unconverted FeF_2 as shown by PDF refinement, suggesting lower reactivity. The coherence PDF scattering domain of Fe^0 was fitted to 2.4 nm, in line with other iron-based electrodes.[18] Remarkably, the transition from

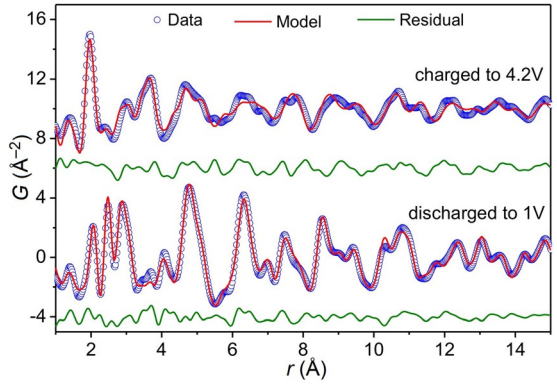

Figure 3. PDF refinements of $FeF_{2.2}(OH)_{0.8-x}O_{x/2}\square_{x/2}$ prepared at 350 °C discharged to 1 V and charged to 4.2 V.

the reduction of Fe^{3+} to Fe^{2+}, to the conversion regime appears smooth. This behavior is characteristic of iron oxyfluoride such as FeOF-type electrodes and is in contrast with pure fluoride (FeF_3 and FeF_2) electrodes.[11,12,19,20]

The charge curves of $FeF_{2.2}(OH)_{0.8-x}O_{x/2}\square_{x/2}$ electrodes show a common feature with a plateau region occurring at 3.5–3.6 V. For $FeF_{2.2}(OH)_{0.8-x}O_{x/2}\square_{x/2}$ prepared at 300 °C, the length of the plateau scales with the conversion domain observed during the discharge process with ~0.7 Li^+. According to PDF analysis, this plateau implies the reaction of LiF and Fe to form an amorphous rutile phase and not the pristine HTB structure. After delithiation, the PDF data show a decrease in intensity due to the disappearance of the strongly scattering metallic phase and concomitant formation of the poorly ordered rutile phase. Similarly, the PDF of the delithiated $FeF_{2.2}(OH)_{0.8-x}O_{x/2}\square_{x/2}$ electrode prepared at 350 °C was fitted using a rutile structure (Figure 3) indicating that this network is the most stable upon re-conversion. Strikingly, the best fit (R_w = 31.6%) was obtained by using two disordered phases of rutile. The presence of a second rutile phase might originate from the fluorine-containing rock salt phase (Li–Fe–O–F) formed upon discharge. The phase transition from rock salt to rutile might explain the additional feature observed in the charge curve of the $FeF_{2.2}(OH)_{0.8-x}O_{x/2}\square_{x/2}$ electrode prepared at 350 °C, that is, a smooth increase in the voltage from 2.7 to 3.2 V with reaction of 0.4 Li^+ per Fe. Further analysis is required to confirm such a hypothesis.

The impact on the electrochemical properties of the nanoscaling/atomic rearrangement induced by discharging electrodes down to 1 V was investigated by cycling $FeF_{2.2}(OH)_{0.8-x}O_{x/2}\square_{x/2}$ electrodes within the 2–4.2 V region. Figure 4 compares the second cycle obtained after performing the first, using a voltage window of either 2–4.2 or 1–4.2 V.

After discharge to 1 V, the $FeF_{2.2}(OH)_{0.8-x}O_{x/2}\square_{x/2}$ electrode prepared at 300 °C shows a much lower capacity than without activation to 1 V. On the other hand, for the $FeF_{2.2}(OH)_{0.8-x}O_{x/2}\square_{x/2}$ electrode prepared at 350 °C, the activation process improves the electrochemical properties relative to the pristine compound, with higher capacity and stable cycling behavior. Additionally, a 90 mV increase of the output voltage over the pristine material was observed, leading to an overall higher energy density. The rationalization of the observed improved electrochemical properties calls for further characterizations, as both rutile and rock salt likely contribute to the electrochemical properties. Additionally, nanoscale features induced by the conversion reaction might be at the origin of the observed enhanced potential.[21]

In summary, the lithium insertion mechanism that occurs in an iron oxyfluoride with varying content of anionic vacancies has been investigated by analyzing the PDFs of electrodes obtained at different states of discharge/charge. The reduction of Fe^{3+} to Fe^{2+} is accompanied by a structural collapse of the HTB framework, yielding a disordered rutile and a rock salt phase. Upon lithiation, the rutile phase is subsequently converted to LiF and Fe^0. The electrochemical activity of $FeF_{2.2}(OH)_{0.8-x}O_{x/2}\square_{x/2}$ electrodes depends on the concentration of anionic vacancies: the higher the vacancy's content, the

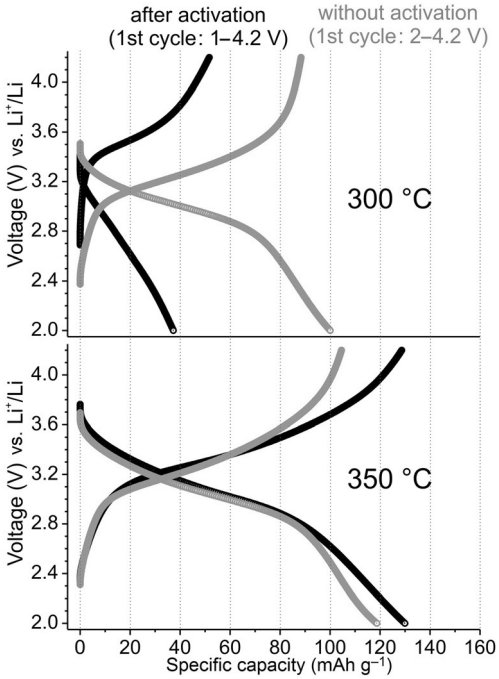

Figure 4. Discharge and charge curves obtained for $FeF_{2.2}(OH)_{0.8-x}O_{x/2}\square_{x/2}$ electrodes prepared at 300 and 350 °C, without (grey) and with (black) activation of the electrode down to 1 V. Cells were cycled under 50 mA g^{-1} within the voltage window of 2–4.2 V.

higher the reversible capacity. Upon delithiation, the pristine HTB structure does not form back, and instead a disordered rutile phase was identified, showing that this structure is the most stable. Furthermore, this study confirms that anionic chemistry dictates the electrochemical activity, that is, anionic partitioning is a common reaction of iron-based oxyfluoride electrodes. Finally, the observed enhanced properties of the electrode after conversion paves the way for a new method toward in-situ-formed new electrode materials.

Experimental Section

Synthesis of iron-based fluoride materials: $FeF_{2.2}(OH)_{0.8}$ was prepared by using a precipitation method assisted by microwave heating as detailed in reference [14]. $FeF_{2.2}(OH)_{0.8}$ was subsequently annealed at 300 and 350 °C for 1 h under Ar, yielding $FeF_{2.2}(OH)_{0.8-x}O_{x/2}\square_{x/2}$ with varied content of anionic vacancies (□).

Electrochemical characterizations: Electrochemical reactions with lithium were performed using coin cells comprising iron-based fluoride and metallic lithium as electrodes. The electrode composition was 75 wt.% active material, 15 wt.% acetylene black as the conductive agent, and 10 wt.% polyvinylidene difluoride as the binder. The various components were hand milled with NMP solvent prior to deposit on aluminum foil. The prepared slurry was spread by a Doctor blade. The area of the electrode was 1.0 cm^2 with a typical mass loading of ~2–3 mg. The electrolyte consists of the commercially available LP30 (1.0 M $LiPF_6$ dissolved in a mixture of ethylene carbonate and ethyl methyl carbonate (3:7 *v/v*). Cells were cycled between 2 and 4.2 V at 50 mA g^{-1} current density.

Pair distribution function (PDF) analysis: Lithiated and delithiated electrodes were recovered in a glove box, washed with DMC and packed in kapton capillaries. High-energy X-ray data were collected at the 11-ID-B station at the Advanced Photon Source (Argonne National Laboratory) using a large amorphous-silicon-based area detector. The data were corrected for background scattering, Compton scattering, and detector effects within pdfgetX2 software. Data were subsequently Fourier transformed to obtain the PDF, $G(r)$.[22] Refinement of the PDF data was performed with PDFgui.[23]

Acknowledgements

Work performed at Argonne and use of the Advanced Photon Source, an Office of Science User Facility operated for the U.S. Department of Energy (DOE) Office of Science by Argonne National Laboratory, were supported by the U.S. DOE under Contract No. DE-AC02-06CH11357. Research leading to these results received funding from the People Programme (Marie Curie Actions) of the European Union's Seventh Framework Programme (FP7/2007–2013) under REA grant agreement no. [321879] (FLUOSYNES) and from the Hydro-Québec Company.

Keywords: anionic partitioning · cathode materials · ferric fluoride · pair distribution function

[1] P. Poizot, S. Laruelle, S. Grugeon, L. Dupont, J. M. Tarascon, *Nature* **2000**, *407*, 496–499.
[2] F. Badway, F. Cosandey, N. Pereira, G. G. Amatucci, *J. Electrochem. Soc.* **2003**, *150*, A1318.
[3] H. Li, G. Richter, J. Maier, *Adv. Mater.* **2003**, *15*, 736–739.
[4] J. Cabana, L. Monconduit, D. Larcher, M. R. Palacin, *Adv. Mater.* **2010**, *22*, E170.
[5] B. Shyam, K. W. Chapman, M. Balasubramanian, R. J. Klingler, G. Srajer, P. J. Chupas, *Angew. Chem. Int. Ed.* **2012**, *51*, 4852–4855; *Angew. Chem.* **2012**, *124*, 4936.
[6] A.-L. Dalverny, J.-S. Filhol, M.-L. Doublet, *J. Mater. Chem.* **2011**, *21*, 10134–10142.
[7] F. Wang, R. Robert, N. A. Chernova, N. Pereira, F. Omenya, F. Badway, X. Hua, M. Ruotolo, R. Zhang, L. Wu, V. Volkov, D. Su, B. Key, M. S. Whittingham, C. P. Grey, G. G. Amatucci, Y. Zhu, J. Graetz, *J. Am. Chem. Soc.* **2011**, *133*, 18828–18836.
[8] F. Lin, D. Nordlund, T.-C. Weng, Y. Zhu, C. Ban, R. M. Richards, H. L. Xin, *Nat. Commun.* **2014**, *5*, 3358.
[9] Y.-S. Hu, Y.-G. Guo, W. Sigle, S. Hore, P. Balaya, J. Maier, *Nat. Mater.* **2006**, *5*, 713–717.
[10] V. L. Chevrier, G. Hautier, S. P. Ong, R. E. Doe, G. Ceder, *Phys. Rev. B: Condens. Matter Mater. Phys.* **2013**, *87*, 094118.
[11] N. Pereira, F. Badway, M. Wartelsky, S. Gunn, G. G. Amatucci, *J. Electrochem. Soc.* **2009**, *156*, A407.
[12] K. M. Wiaderek, O. J. Borkiewicz, E. Castillo-Martínez, R. Robert, N. Pereira, G. G. Amatucci, C. P. Grey, P. J. Chupas, K. W. Chapman, *J. Am. Chem. Soc.* **2013**, *135*, 4070–4078.
[13] D. Dambournet, K. W. Chapman, P. J. Chupas, R. E. Gerald, C. Labrugere, A. Demourgues, A. Tressaud, K. Amine, *J. Am. Chem. Soc.* **2011**, *133*, 13240–13243.
[14] M. Duttine, D. Dambournet, N. Penin, D. Carlier, L. Bourgeois, A. Wattiaux, K. W. Chapman, P. J. Chupas, H. Groult, E. Durand, A. Demourgues, *Chem. Mater.* **2014**, *26*, 4190–4199.
[15] C. Li, L. Gu, J. Tong, S. Tsukimoto, J. Maier, *Adv. Funct. Mater.* **2011**, *21*, 1391–1397.
[16] T. Egami, S. J. L. Billinge in *Underneath the Bragg Peaks: Structural Analysis of Complex Materials* (Ed.: R. Cahn), Pergamon Press, Oxford **2004**.
[17] Y.-N. Zhou, M. Sina, N. Pereira, X. Yu, G. G. Amatucci, X.-Q. Yang, F. Cosandey, K.-W. Nam, *Adv. Funct. Mater.* **2015**, *25*, 696–703.
[18] K. M. Wiaderek, O. J. Borkiewicz, N. Pereira, J. Ilavsky, G. G. Amatucci, P. J. Chupas, K. W. Chapman, *J. Am. Chem. Soc.* **2014**, *136*, 6211–6214.

[19] N. Yamakawa, M. Jiang, B. Key, C. P. Grey, *J. Am. Chem. Soc.* **2009**, *131*, 10525 – 10536.
[20] J. K. Ko, K. M. Wiaderek, N. Pereira, T. L. Kinnibrugh, J. R. Kim, P. J. Chupas, K. W. Chapman, G. G. Amatucci, *ACS Appl. Mater. Interfaces* **2014**, *6*, 10858 – 10869.
[21] O. Delmer, P. Balaya, L. Kienle, J. Maier, *J. Adv. Mater.* **2008**, *20*, 501 – 505.
[22] X. Qiu, J. W. Thompson, S. J. L. Billinge, *J. Appl. Crystallogr.* **2004**, *37*, 678 – 678.
[23] C. L. Farrow, P. Juhás, J. W. Liu, D. Bryndin, E. S. Božin, J. Bloch, Th. Proffen, S. J. L. Billinge, *J. Phys. Condens. Matter* **2007**, *19*, 335219.

Received: February 2, 2015
Published online on June 25, 2015

